

1 **Mechanisms and effects of under-ice warming water in Ngoring**
2 **Lake of Qinghai-Tibet Plateau**

3 Mengxiao Wang ^{1,2}, Lijuan Wen ^{1*}, Zhaoguo Li ¹, Matti Leppäranta ³,
4 Victor Stepanenko ^{4,5}, Yixin Zhao ^{1,2}, Ruijia Niu ^{1,2}, Liuyiyi Yang ^{1,2} and
5 Georgiy Kirillin ⁶

6 ¹ Key Laboratory of Land Surface Process and Climate Change in Cold and Arid
7 Regions, Northwest Institute of Eco-Environment and Resources, Chinese Academy of
8 Sciences, 730000 Lanzhou, China

9 ² University of Chinese Academy of Sciences, 10049 Beijing, China

10 ³ Institute of Atmospheric and Earth Sciences, University of Helsinki

11 ⁴ Research Computing Center, Lomonosov Moscow State University, Moscow, Russia

12 ⁵ Moscow Center for Fundamental and Applied Mathematics, Moscow, Russia

13 ⁶ Department of Ecohydrology, Leibniz-Institute of Freshwater Ecology and Inland
14 Fisheries (IGB), Berlin, Germany

15 **Correspondence to: Lijuan Wen (wlj@lzb.ac.cn)*

16
17 **Abstract** The seasonal ice cover in lakes of the Qinghai-Tibet Plateau is a transient and
18 vulnerable part of the cryosphere, whose characteristics depend on the regional climate:
19 strong solar radiation in the context of the dry and cold environment because of high-
20 altitude and relatively low-latitude. We use the first under-ice temperature observations
21 from the largest Tibetan freshwater lake Ngoring and a one-dimensional lake model to
22 quantify the mechanism of solar thermal accumulation under ice, which relies on the
23 ice optical properties and weather conditions, as well as the effect of the accumulated
24 heat on the land-atmosphere heat exchange after the ice break-up. The model was able
25 to realistically simulate the feature of Ngoring Lake thermal regime: the “summer-like”
26 temperature stratification with temperatures exceeding the maximum density point of
27 3.98 °C across the bulk of the water column. A series of sensitivity experiments revealed
28 solar radiation was the major source of under-ice warming and demonstrated that the
29 warming phenomenon was highly sensitive to the optical properties of ice. The heat
30 accumulated under ice contributed to the heat release from the lake to the atmosphere
31 for 1-2 months after ice-off, increasing the upward sensible and latent surface heat
32 fluxes on average by $\sim 50 \text{ W m}^{-2}$ and $\sim 80 \text{ W m}^{-2}$, respectively. Therefore, the delayed
33 effect of heat release on the land-atmosphere interaction requires an adequate

34 representation in regional climate modeling of the Qinghai-Tibet Plateau and other
35 lake-rich alpine areas.

36

37 **1 Introduction**

38 Seasonal lake ice is a part of the cryosphere, gaining recent attention from
39 researchers due to its sensitivity to climate change (Kirillin et al., 2012; Sharma et al.,
40 2020). The duration of ice cover affects the stability and vertical mixing of lakes, as
41 well as the lake-atmosphere matter and energy exchange (Rösner et al., 2012; Efremova
42 et al., 2013; Ramp et al., 2015). Ice cover regulates lake biochemical indicators, such
43 as the concentration of dissolved oxygen, nitrogen, and phosphorus, changing the
44 biochemical reaction rate and affecting the water quality and distribution of aquatic
45 organisms (Weitere et al., 2010; Dokulil, 2013; Li et al., 2015a; Hardenbicker et al.,
46 2016). Shortening of the ice season has been observed worldwide (Sharma et al., 2019;
47 Dauginis and Brown, 2021) and attributed to anthropogenic warming (Grant et al.,
48 2021). Future climate predictions indicated the accelerated reduction of seasonal lake
49 ice, especially pronounced in the lake-rich Arctic regions (Brown and Duguay, 2011).
50 Global assessment of seasonal lake ice changes requires quantification of the major heat
51 sources and sinks on seasonal to climatic time scales. While the major prerequisite for
52 the ice cover development is sufficient long season with air temperature below the
53 freezing point of water, the heat budget of ice-covered lakes varies with latitude and
54 altitude, depending strongly on the available solar radiation, the latter being the major
55 source of heat for under-ice lake water (Kirillin et al., 2012). During the polar night in
56 the Arctic and temperate lakes covered by snow, the solar heating is minor and the
57 bottom sediment is the main heat source (Winter I according to Kirillin et al., 2012); at
58 later stages of the ice season (Winter II), as the snow melts, solar radiation becomes to
59 the main heat source governing thermal stratification and mixing under ice and the
60 melting process at the ice base (Kirillin et al., 2018, 2020). Further, lakes with seasonal
61 ice cover can be divided into cryomictic and cryostratified according to their maximum
62 depth, surface area, and wind speed (Yang et al., 2021). In dry and cold areas with little
63 snow, winter II can occupy the entire ice-covered period (Kirillin et al., 2012), making
64 solar radiation to be the major factor affecting the lake ice regime. The situation is
65 relevant to the alpine lakes.

66 In particular, the largest alpine lake system of the Qinghai-Tibet Plateau (TP), is
67 not only the highest plateau on Earth with an average altitude of 4000-5000 m, but also
68 located in the relatively low-latitude of 26-39° N ensures a high amount of solar
69 radiation. The TP is covered by more than 1400 lakes with an area larger than 1 km²,

70 and the total lake area is more than 5×10^4 km², accounting for 57.2 % of that in China
71 (Wan et al., 2016; Zhang et al., 2019). Recent studies reported the first observations
72 from ice-covered Tibetan lakes, indicating the major role of solar radiation in their
73 thermal regime (Wang et al., 2021). Water temperatures in Lakes Bangong Co and Nam
74 Co constantly increased during the ice-covered period, with a stronger increase in
75 shallower Bangong Co (Lazhu et al., 2021). Observations in meromictic Dagze Co Lake
76 demonstrated stable temperature in the early ice-covered period start warming only in
77 the late ice-covered period, conditioned by the high water salinity (Wang et al., 2014;
78 Lazhu et al., 2021). Salinity has a strong influence on the temperature and mixing
79 regime of all three abovementioned lakes, by altering their density stratification and
80 vertical heat transport. Among freshwater lakes in the TP, Ngoring Lake is the largest
81 one (Kirillin et al., 2017; Wen et al., 2022). Kirillin et al. (2021) found strong solar
82 radiation under ice cover heating the entire lake water column to the maximum
83 freshwater density temperature (~ 3.98 °C, T_{md}) more than a month before the ice
84 breakup—the situation never found in lowland freshwater lakes. As a result, strong heat
85 release from water to the ice base turned into the major factor governing the ice melt,
86 with the water temperature under ice achieving 6 °C. This radiation-dominated regime,
87 differing dramatically from the typical heat budget known from earlier studies on ice-
88 covered lakes. Although it belongs to the classification that winter II occupies the whole
89 ice-covered period, the under-ice lake temperature exceeds 4 °C in the late stage due to
90 the strong SR on the TP. Quantification of the resulting heat balance and thermal
91 stratification characteristic of alpine conditions is the subject of the present study.

92 Due to the harsh environment of the TP and difficulties in collecting field
93 observations, numerical models are often used to investigate phenomena and
94 mechanisms of TP lakes. At present, the widely used lake models are the FLake model
95 and the lake scheme coupled in the CLM (Community Land Model), CoLM (Common
96 Land Model), and WRF (Weather Research and Forecasting Model) (Lazhu et al., 2016;
97 Wen et al., 2016; Fang et al., 2017; Dai et al., 2018; Huang et al., 2019; Song et al.,
98 2020; Wu et al., 2021). However, for computational efficiency, winter dynamics in these
99 highly-parameterized lake models are represented in a rather simplified way, lacking
100 the detailed mechanisms of heating by radiation and resulting vertical heat transports
101 across the water column (Lazhu et al., 2016; Wen et al., 2016; Huang et al., 2019). As
102 an alternative, we adopt for this study a “classical” two-equation turbulence modeling
103 approach proving its reliability in decades of studies on the environmental turbulent
104 fluid dynamics. The one-dimensional model LAKE implements the approach in
105 application to lake dynamics and was applied previously to different lakes (Stepanenko
106 et al., 2011, 2016; Guseva et al., 2016). We combine modeling with in situ observations
107 from Ngoring Lake, data on weather forcing and remote sensing to: (i) test the ability

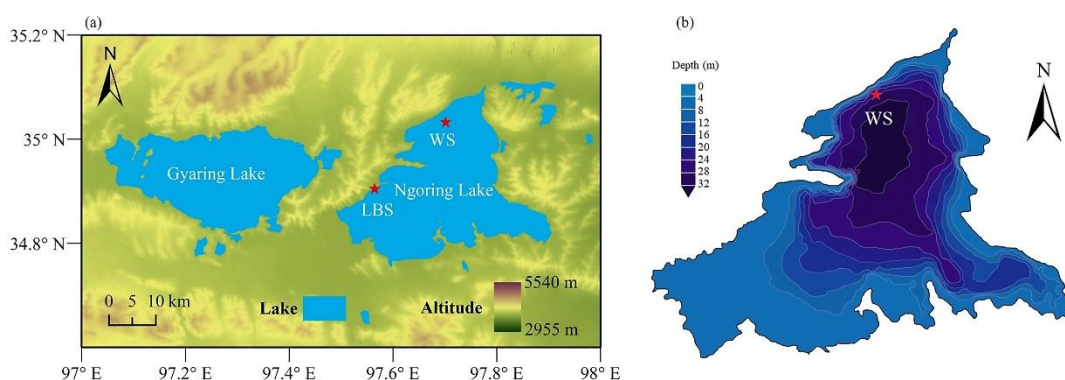
108 of a one-dimensional lake model LAKE to simulate temperature and stratification
109 driven by intense solar heating in ice-covered Lake Ngoring; (ii) conduct series of
110 sensitivity experiments aimed at revealing the role of meteorological forcing and ice
111 optical properties in lake temperature and mixing regime; and (iii) reveal the effects of
112 temperature distribution before ice breakup on lake heat storage and lake-atmosphere
113 heat transfer.

114

115 2 Study area and data

116 2.1 Study area

117 Ngoring Lake (34.76-35.08° N, 97.53-97.90° E, Fig. 1) is located in the western
118 valley of Maduo County on the eastern TP, with an average lake surface elevation of
119 4274 m a.s.l. It is the largest freshwater lake in the Yellow River source region with a
120 salinity of about 0.27 g kg⁻¹ (Shen et al., 2012). It has a surface area of 610 km², a
121 maximum depth of 32 m, and an average depth of 17 m. The pH is 8.49 and there are
122 very few fish in the lake. Aquatic plants grow only in the riparian area. The lake
123 thermally stratifies in summer and is covered by ice from late November or early
124 December to late April (Wen et al., 2016). According to observational data from 1953
125 to 2016 at Maduo station (34.9° N, 98.2° E) of the China Meteorological Administration,
126 the average annual precipitation was 322.4 mm, mostly concentrated from May to
127 September. The average annual air temperature was -3.53 °C. The maximum air
128 temperature was 24.3 °C occurred on July 20, 2006, and the minimum air temperature
129 was -48.1 °C occurred on January 2, 1978.



130

131 **Figure 1. (a) Location and (b) bathymetry of Ngoring Lake. (b) is adapted from**
132 **Kirillin et al., 2021. The pentagrams denote the lake border station (LBS) and**
133 **water temperature measurement site (WS).**

134

135 **2.2 Data**

136 **2.2.1 Observations: LBS station and WS site**

137 The long-term automatic lake border station (LBS, 34.91° N, 97.55° E, Fig. 1) was
138 installed in October 2012, with an altitude of 4282 m a.s.l., providing meteorological
139 forcing data: wind speed at 10 m, air temperature, specific humidity and air pressure at
140 2 m, downward shortwave (SR) and longwave radiation (LR) at 1.5 m from September
141 2015 to September 2016 (Li et al., 2020). The detailed information about site
142 configuration and measured quantities are referred to in Li et al. (2015b) and Wen et al.
143 (2016). The precipitation was obtained from the daily value data set (V3.0) at Maduo
144 station of Chinese surface climate data (<http://data.cma.cn>).

145 The water temperature measurement site (WS, 35.03° N, 97.70° E, Fig. 1) was
146 located in the northern of Ngoring Lake, where the total water depth was about 26.5 m.
147 The multi-layer water temperature observation system consisted of 16 self-recording
148 RBR SOLO water temperature probes with a precision of 0.01 °C. The sampling
149 distance and time intervals were 1 m and 10 minutes, respectively.

150

151 **2.2.2 MODIS lake surface temperature**

152 The 8-day L3 global lake surface temperature product (MYD11C2) was derived
153 from the data of Moderate Resolution Imaging Spectroradiometer (MODIS) and was
154 used to evaluate the simulated results. MODIS offers long-term daily global coverage
155 data with high spatial resolution. This product provides an 8-day combined radiative
156 surface temperature at approximately 10:30 and 22:30 LT (local time), which is the
157 satellite transit time. The resolution is 0.05° latitude/longitude (5600 m at the equator)
158 for Climate Modeling Grid (CMG) (<https://ladsweb.nascom.nasa.gov/search>) (Wan et
159 al., 2004).

160

161 **2.2.3 ERA5-Land data**

162 ERA5-Land is produced as an enhanced global dataset for the land component of
163 the fifth generation of European ReAnalysis (ERA5) by the European Centre for
164 Medium-Range Weather Forecasts (ECMWF), framed within the Copernicus Climate
165 Change Service (C3S) of the European Commission. It is available for ERA5-Land
166 hourly record for about 40 years from 1981 to the present. Expediently, ERA5-Land
167 has an enhanced horizontal resolution of 9 km (~0.08°) compared to ERA5 (31 km) and
168 ERA-Interim (80 km) (<https://cds.climate.copernicus.eu/cdsapp#!/dataset/reanalysis->

169 era5-land?tab=form) (Hersbach et al., 2020; Muñoz-Sabater et al., 2021).

170 ERA5-Land data is applied for a comparative analysis of warming mechanisms
171 and thermal conditions in Tibetan ice-covered lakes against those in the Arctic. The
172 reanalysis forcing data for the geographical position 69.05° N, 20.83° E was adopted as
173 “typical” arctic weather conditions, that is, the SR is 0 W m⁻² during the winter polar
174 night period. Northern Fennoscandia is covered by several lakes characterized by the
175 longest ice-covered period in Western Europe. The largest of these lakes, Kilpisjärvi,
176 has a similar morphometrical feature to Ngoring (average depth 19.5 m, maximum
177 depth 57 m, surface area 37 km²). However, they receive different SR because of
178 different latitudes. The lake has been intensively studied in the last decades (Kirillin et
179 al., 2015, 2018; Leppäranta et al., 2017, 2019). Its under-ice water temperature
180 remained stable during winter from 1992 to 1993 (Tolonen, 1998). In the following,
181 model experiments forced by the ERA5 weather data (1992-1993) for the Arctic refer
182 to “Kilpisjärvi” runs.

183

184 **3 Methods**

185 **3.1 LAKE model**

186 The one-dimensional model LAKE, simulating thermodynamic, hydrodynamic,
187 and biogeochemical processes, is used to solve the horizontally averaged transfer of
188 gases, heat, salts, and momentum in an enclosed water body (Stepanenko et al., 2011,
189 2016). The vertical heat diffusion is simulated, and the penetration of solar radiation
190 into the water ice, snow, and bottom sediments layers (Heiskanen et al., 2015; Cao et
191 al., 2020) is taken into account. The exchange between the water and the inclined
192 bottom is modeled explicitly because the model equations have been averaged over
193 horizontal sections of the water body. The 2nd order κ - ϵ parametrization of turbulence
194 is applied (Stepanenko et al., 2016).

195

196 **3.1.1 Heat transfer in water body**

197 The water temperature is calculated according to the one-dimensional thermal
198 diffusion equation:

$$\begin{aligned} 199 \quad c_w \rho_w \frac{\partial T_w}{\partial t} = & -c_w \rho_w \frac{1}{A} \int_{\Gamma_A} T_w (u_h \cdot n) dl + \frac{1}{Ah^2} \frac{\partial}{\partial \xi} \left(A_w K_T \frac{\partial T_w}{\partial \xi} \right) - \frac{1}{Ah} \frac{\partial AS}{\partial \xi} + \\ 200 \quad & \frac{1}{Ah} \frac{\partial A}{\partial \xi} [S_b(\xi) + F_{iz,b}(\xi)] + \frac{dh}{dt} \frac{\xi}{h} \frac{\partial T_w}{\partial \xi}, \quad (1) \end{aligned}$$

201 where c_w is water specific heat, ρ_w is water density, T_w is water temperature, $h(t)$ is

202 lake depth, t is time, $\xi = z/h$ is a normalized vertical coordinate ($z \in [0, h]$), $z = 0$ is
 203 located at the free water surface of the lake, S is downward shortwave radiation, A_w is
 204 the z -dependent cross-sectional area of water, K_T is thermal diffusivity coefficient
 205 equal to the sum of molecular and turbulent diffusivities, $S_b(\xi)$ is shortwave radiation
 206 flux, $F_{i,z,b}$ is soil heat flux at the level z , n is an outer normal vector to the boundary Γ_A
 207 of the horizontal cross-section A and u_h is horizontal vector in water (Stepanenko et al.,
 208 2016; Guseva et al., 2016).

209

210 3.1.2 Heat transfer in ice cover

211 When the air temperature decreases below 0 °C and the surface water temperature
 212 drops to the freezing point, the initial ice cover forms. When the net radiation of the
 213 lake is positive, the ice melts continuously until the ice thickness declines to zero. The
 214 general heat conduction equation in ice cover follows the equation:

$$215 \quad c_i \rho_i \frac{\partial T_i}{\partial t} = c_i \rho_i \frac{\xi}{h_i} \frac{dh_i}{dt} \frac{\partial T_i}{\partial \xi} - c_i \rho_i \frac{1}{h_i} \frac{dh_{i0}}{dt} \frac{\partial T_i}{\partial \xi} - \frac{1}{h_i} \frac{\partial S}{\partial \xi} + \frac{1}{A_i h_i^2} \frac{\partial}{\partial \xi} \left(A_i \lambda_i \frac{\partial T_i}{\partial \xi} \right) + \frac{1}{A_i h_i} \frac{\partial A_i}{\partial \xi} F_{T,b} -$$

$$216 \quad L \rho_i \frac{dp}{dt} , \quad (2)$$

217 where c_i is ice specific heat, ρ_i is ice density, T_i is ice temperature, λ_i is ice thermal
 218 conductivity, h_i is ice thickness, $\frac{dh_{i0}}{dt}$ is the increment of ice thickness on its surface,
 219 $F_{T,b}$ is the heat flux at the ice-sediment boundary, A_i is the z -dependent cross-sectional
 220 area of the ice cover determined by the basin morphometry, L is the latent heat of water
 221 and p is ice porosity (Stepanenko et al., 2019). The last term to the right-hand side
 222 presents heat of phase transition of salty water in ice pores.

223 The penetration of solar radiation into the medium is calculated using the Beer-
 224 Lambert law (Stepanenko and Lykossov, 2005; Stepanenko et al., 2019):

$$225 \quad S(\xi) = S(0) \exp(-a_e h \xi) , \quad (3)$$

226 where a_e is the medium extinction coefficient. To solve the temperature in Eq. (1 & 2),
 227 it is necessary to specify the top and bottom boundary conditions and provide the
 228 method to calculate the heat flux at each depth z . The atmospheric turbulent heat flux
 229 schemes are based on the Monin-Obukhov similarity theory (Stepanenko et al., 2016).

230 When the lake is covered by ice, the temperatures of the bottom layer of ice and
 231 the top layer of water are equal and fixed to the melting/freezing point temperature
 232 (Stepanenko et al., 2019), which is calculated by the following formula:

$$233 \quad T_{mp} = -C * \left| \frac{\partial T_{mp}}{\partial C} \right| , \quad (4)$$

234 where T_{mp} is the melting/freezing point temperature (°C), C is salinity at the water-
 235 ice interface, $\left| \frac{\partial T_{mp}}{\partial C} \right| = 66.7$ is assumed constant.

236 Based on the study by Leppäranta (2014), the albedo regulates the surface energy
 237 budget, and the extinction coefficient controls the vertical distribution of radiation
 238 energy in the medium. In the LAKE model, the albedo of water (A_w) is 0.06, and the
 239 snow extinction coefficient (E_s) decreases with increased snow density. Snow
 240 accumulation in the Ngoring Lake area is almost zero. Therefore, only A_i , E_i , and E_w
 241 are analyzed in this study. Version 2.3 called LAKE2.3 is used in this article.

242

243 **3.2 Methods to evaluate the model accuracy**

244 The indexes to evaluate accuracy of the model are the root mean square error
 245 ($RMSE$), $BIAS$, and correlation coefficient (CC):

$$246 \quad RMSE = \sqrt{\frac{1}{n} \sum_{j=0}^n (m_j - o_j)^2} , \quad (5)$$

$$247 \quad BIAS = \bar{m} - \bar{o} , \quad (6)$$

$$248 \quad CC = \frac{\text{Cov}(M,O)}{\sqrt{\text{Var}(M)\text{Var}(O)}} , \quad (7)$$

249 where m_j and o_j represent the simulations and observations. \bar{m} and \bar{o} are the
 250 corresponding average values. $\text{Var}(M)$ and $\text{Var}(O)$ are the variances of observed and
 251 simulated values, respectively. $\text{Cov}(M, O)$ is the covariances.

252

253 **3.3 Calculation method of heat storage**

254 The heat storage evolution in water is calculated by the following formulation:

$$255 \quad Q = c_w \rho_w \sum_{k=1}^n T_k \Delta z_k , \quad (8)$$

256 where $c_w = 4192 \text{ J kg}^{-1} \text{ K}^{-1}$ and $\rho_w = 10^3 \text{ kg m}^{-3}$, n is the layer number, Δz_k is depth
 257 interval between two successive layers and T_k (K) is the average temperature in layer k
 258 (Nordbo et al., 2011; Gan and Liu, 2020).

259

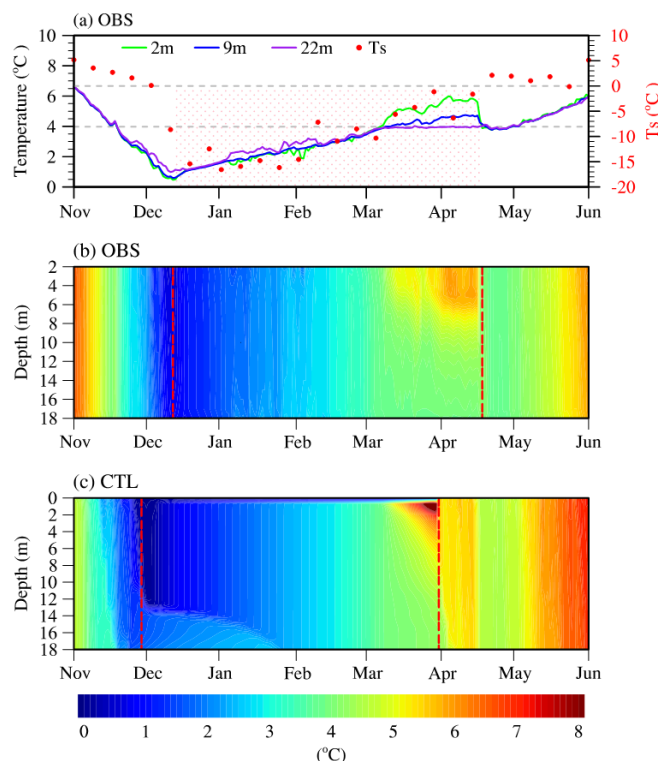
260 **4 Characteristic analysis of water temperature and local climate in two lakes**

261 **4.1 Characteristics of water temperature**

262 It is pointed out that the under-ice water temperature from 2015 to 2016 in Ngoring
 263 Lake rose continuously during the entire ice-covered period according to observations
 264 (Wang et al., 2021; Kirillin et al., 2021). In November, because of the strong wind and

265 wide surface, the lake mixed evenly with slight oscillation (<1 °C between 2 m and 22
 266 m) and water temperature decreased gradually until the lowest point of 0.47 °C at 2 m
 267 on December 12, the lake froze up completely (Fig. 2a). Meanwhile, the 2 m air
 268 temperature fell to -7.79 °C. Ngoring Lake is mostly covered only by bare ice in winter
 269 due to drought, less precipitation and snow. In the early ice-covered phase (from
 270 December 12 to March 7), the whole lake mixed completely because solar radiation
 271 penetrated ice and heated the upper water, which was warm ($< T_{md}$), heavy and sinking
 272 (Fig. 2b) (Kirillin et al., 2012). In parallel, water temperature continued to warm until
 273 reached T_{md} on March 7 (Fig. 2a).

274 In the late ice-covered stage (from March 7 to April 18), the lake stratified. On the
 275 one hand, owing to solar radiation strengthened, on the other hand, since radiation
 276 absorption of water decayed with depth based on the Beer-Lambert law. Water
 277 temperature increased at the rate of 0.052 °C d^{-1} in the layers from 2 m to 6 m, which
 278 was more rapid than the early stage of 0.035 °C d^{-1} . On April 18, the ice melted entirely
 279 as well water temperature rose to 5.83 °C at 2 m while remaining at T_{md} below 9 m.
 280 After that, full mixing took place rapidly because the lake warmed gaining heat from
 281 the sun and atmosphere as a result of ice breaking up (Fig. 2b).



282
 283 **Figure 2. (a) The daily average water temperature observations of Ngoring Lake**
 284 **at the surface (T_s), 2 m, 9 m, and 22 m from November 1, 2015 to June 1, 2016. T_s**
 285 **is MODIS lake surface temperature. The gray reference lines denote 3.98 °C and**
 286 **0 °C, respectively. The pink shaded area denotes ice-covered period. The water**

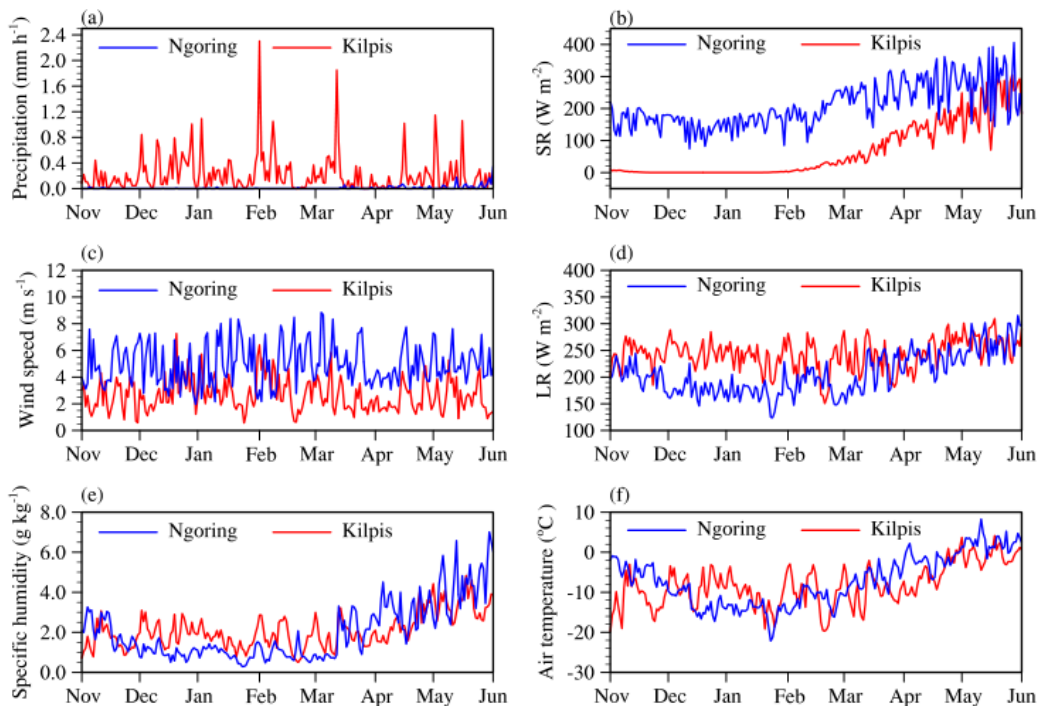
287 temperature profile (b) observed and (c) simulated in CTL. The ice-covered period
 288 is represented between the two red dashed lines.

289

290 4.2 Local climate: Tibet vs. Kilpisjärvi

291 The daily averages of meteorological variables between Tibet and Kilpisjärvi were
 292 shown in Fig. 3, the ranges and averages of that during the ice-covered period (from
 293 December 12 to April 18 based on Ngoring Lake) were compared (Table 1). The
 294 average differences in air temperature, specific humidity, and downward LR were -
 295 0.42 °C, -0.38 g kg⁻¹, and 41.9 W m⁻², respectively. The wind speed of Tibet was 1.7
 296 times that of Kilpisjärvi, and the downward SR in Tibet of 199.41 W m⁻² was stronger
 297 than in Kilpisjärvi of 40.46 W m⁻². The precipitation was a multiple of 0.037 in Tibet
 298 than that in Kilpisjärvi.

299 On the whole, there were few differences in air temperature, specific humidity, and
 300 downward LR in the two regions. Nevertheless, there was much lower precipitation,
 301 much higher downward SR and wind speed in the high-altitude and relatively low-
 302 latitude Tibet. Surface pressure was not considered in this study since the little effect
 303 on water temperature.



304

305 **Figure 3. Comparison of daily average values of the meteorological variables for**
 306 **Tibet from 2015 to 2016 and for Kilpisjärvi from 1992 to 1993. (a) precipitation,**
 307 **(b) downward SR, (c) wind speed, (d) downward LR, (e) specific humidity, and (f)**
 308 **air temperature. The “Ngoring” represents the Tibet region and the “Kilpis”**
 309 **represents Kilpisjärvi region.**

310 **Table 1.** Ranges and averages of the meteorological variables of Tibet (2015-2016)
 311 compared with Kilpisjärvi (1992-1993) during the ice-covered period (12.12-4.18).

Meteorologic variables	Tibet		Kilpisjärvi	
	Range	Average	Range	Average
Precipitation (mm h ⁻¹)	< 0.072	0.0044	< 1.15	0.12
Downward SR (W m ⁻²)	73.98-356.29	199.41	< 186.84	40.46
Wind speed (m s ⁻¹)	1.95-8.85	4.93	0.56-7.28	2.83
Downward LR (W m ⁻²)	123.92-271.60	191.73	150.61-289.59	233.62
Specific humidity (g kg ⁻¹)	0.29-4.52	1.40	0.50-3.23	1.78
Air temperature (°C)	-22.16-2.24	-10.25	-19.69-2.01	-9.83

312

313 **5 Simulation setup**

314 To reveal the mechanism of water temperature rising during ice-covered period in
 315 Ngoring Lake and its further influences, one control simulation (CTL) and 27
 316 sensitivity simulations (SIM) depending on CTL were set in this study (Table 2).

317

318 **5.1 Setup in CTL**

319 The depth was set as 26.5 m, measured at the WS point, and divided vertically into
 320 35 layers. The simulation period was from September 2015 to September 2016. The
 321 initial vertical profile of water temperature, mixed layer, and the bottom temperature
 322 were set following the observations (Fig. 2b). The albedos of snow and ice and the
 323 extinction coefficients of ice and water were set as $A_s = 0.7$, $A_i = 0.25$, $E_i = 2.5 \text{ m}^{-1}$, and
 324 $E_w = 0.15 \text{ m}^{-1}$ based on previous investigations (Lei et al., 2011; Li et al., 2018, 2020;

325 Shang et al., 2018). The input driving meteorological variables were air pressure, wind
 326 speed, specific humidity, air temperature, precipitation, downward SR and LR. The
 327 forcing data and model run intervals were 30 minutes and 15 seconds respectively.

328

329 5.2 Setup in SIM

330 To explore the influence of a single meteorological variable, SIM_* simulations
 331 were set up. The symbol * is SR, Precip, LR, U, T_{air} , or q in Kilpisjärvi. These scenarios
 332 were quite artificial because these variables are closely correlated. Despite that, these
 333 sensitivity simulations can shed light on the influence of local climate on lake
 334 temperature evolution during ice-covered period.

335 To discuss the effect of main physical parameters, SIM_# simulations were set up,
 336 the sign # represented the values of A_i , E_i , or E_w . SIM_E* (* equal to 1, 2, or 3) is set
 337 for exploring the effects of three different initial water temperature profiles before ice
 338 breakup on the lake heat storage and heat fluxes.

339

340 **Table 2.** Names, explanations, and amounts of all experiments.

Experiment name	Experiment explanation	Amount
CTL	The control simulation	1
SIM_*		
(* represents meteorological variables)	The simulation when the * variable is replaced by that of Kilpisjärvi.	6
SIM_#		
(# represents values of A_i , E_i or E_w)	The simulation when the corresponding physical variable is equal to #, respectively.	18
SIM_E*		
(* represents 1, 2, and 3)	The simulation when using three different initial temperature profiles before ice melting based on CTL.	3

341

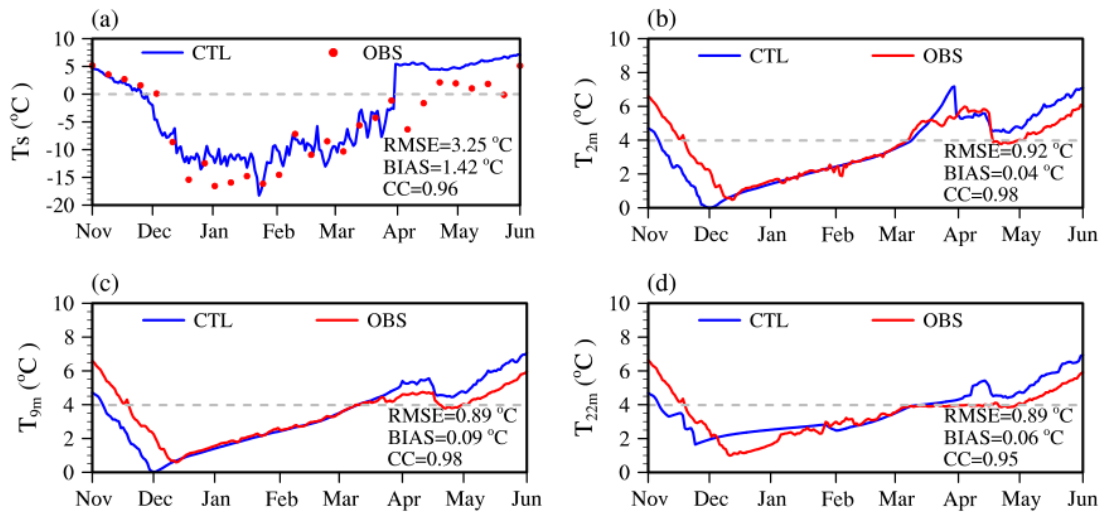
342 6 Simulation results

343 6.1 Model validation

344 The CTL simulation was relatively consistent with the observations (Fig. 2b,c),

345 even though the whole ice season advanced by about 15 days than observed. Water
 346 temperature was a little higher in CTL than that in the observations from mid-March to
 347 late May. The deviation was greater in the deep water. The simulated temperature
 348 warmed faster and higher by 1 °C than the observed value after ice melted.

349 The results were evaluated by calculating *RMSE*, *BIAS*, *CC* between simulated and
 350 observed water temperature at the lake surface (T_s), 2 m, 9 m and 22 m (Fig. 4). The
 351 *CC* in each layer was equal to even greater than 0.95, and the *CC* in 2 m and 9 m are as
 352 high as 0.98, even though *RMSE* and *BIAS* of lake surface were 3.25 °C and 1.42 °C,
 353 respectively. The T_s *RMSE* was largely due to the uncertainty of MODIS lake surface
 354 temperature (Donlon et al., 2002; Tavares et al., 2019). The *BIAS* absolute values in the
 355 internal lake were less than 0.01 °C, and *RMSE* was less than 0.95 °C. More important,
 356 the under-ice water temperature warming phenomenon was reproduced reasonably.



357

358 **Figure 4. The daily average water temperature observed and simulated in CTL of**
 359 **(a) the surface (T_s), (b) 2 m, (c) 9 m, (d) 22 m in Ngoring Lake from November**
 360 **2015 to June 2016. The dotted lines represent T_{md} 3.98 °C.**

361

362 6.2 Influences of local climate on water temperature

363 To explore the influences of local climate on water temperature, six simulations
 364 SIM_* (* represents 6 meteorological variables, Table 2) were designed. The 3 m water
 365 temperature was typically selected to analyze since water temperature at different
 366 depths varied consistently over time.

367 SIM_SR was the simulation when the Kilpisjärvi downward SR was substituted
 368 for that in Tibet. During the ice-covered period, the downward SR difference between
 369 CTL (199.41 W m⁻²) and SIM_SR (40.46 W m⁻²) was 158.95 W m⁻². In the sensitivity
 370 simulation SIM_SR, the 3 m water temperature was stable keeping in the range of 0-

371 0.1 °C (Fig. 5a). The ice formation date was earlier and the ice-breaking date delayed,
372 which led to the growth of the whole ice season. The mixed layer depth increased (Fig.
373 5d). Consequently, the strong downward SR on the TP generated the under-ice water
374 warming in Ngoring Lake.

375 In the simulation SIM_Precip, the Tibet precipitation was replaced by that in
376 Kilpisjärvi. In the sensitivity experiment SIM_Precip, the 3 m water temperature fixed,
377 then increased but did not exceed T_{md} in the early ice cover stage (Fig. 5a). The
378 stratification and temperature maximum center disappeared in late March, and the lake
379 was fully mixed (Fig. 2c,5g). Because the average precipitation in SIM_Precip (0.12
380 mm h⁻¹) was approximately 30 times larger than that in CTL (0.0044 mm h⁻¹) during
381 ice-covered period, more solar radiation was reflected and absorbed by snow due to
382 more snowfall accumulation. Thus, the high precipitation damped the water
383 temperature rise.

384 In SIM_LR simulation, the downward LR in Kilpisjärvi superseded that in Tibet.
385 The average downward LR was 233.62 W m⁻² in SIM_LR, which was stronger than
386 that in CTL (191.73 W m⁻²) during ice-covered period. The 3 m water temperature still
387 warmed as well the complete ice melting time of late February was ahead. The heat was
388 transferred from lake to atmosphere because of lower air temperature after ice breakup.
389 The water temperature underwent a cooling process (2 °C) until reaching a new
390 equilibrium with atmosphere (Fig. 5b). Compared with the CTL, water mixing in the
391 ice-covered period was more uniform, the stratification in late March was weakened,
392 and the temperature maximum center advanced about 15 days (Fig. 5e).

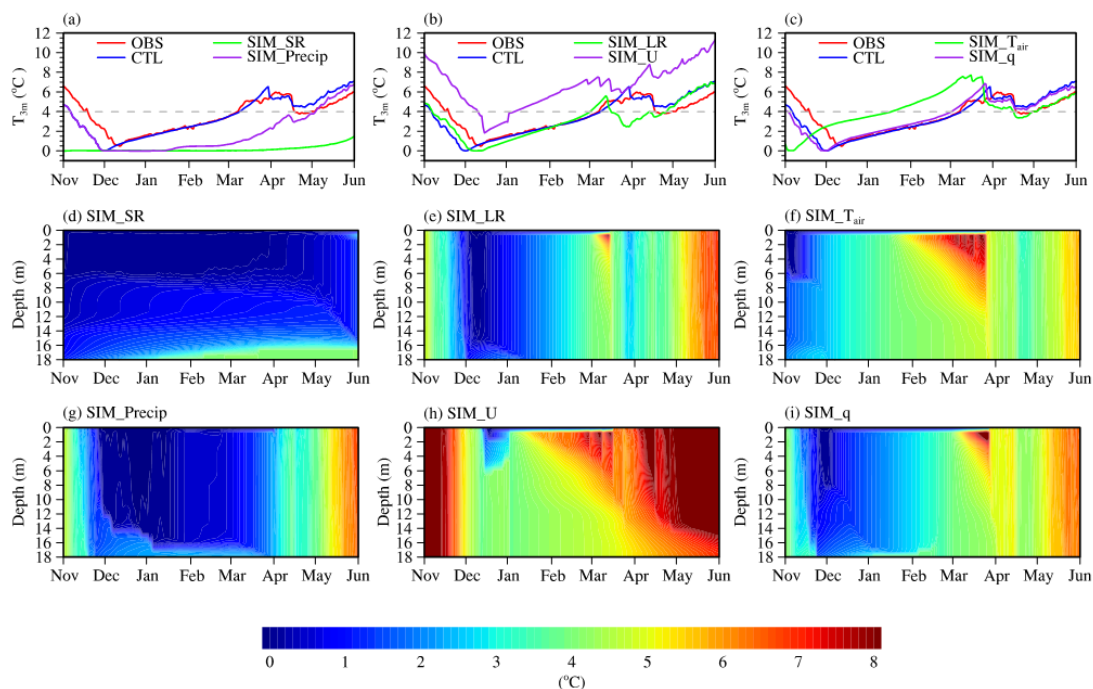
393 In SIM_U simulation, the wind speed of Kilpisjärvi was substituted for that of Tibet.
394 The wind speed in SIM_U (2.83 m s⁻¹) was weaker than that in CTL (4.93 m s⁻¹) for the
395 ice-covered period. In the sensitivity experiment SIM_U, the 3 m water temperature
396 kept rising, but it was about 3 °C higher than that in CTL during the whole simulation
397 period (Fig. 5b). Due to the decrease in wind speed, the mixed layer depth was reduced,
398 and the lake stratification was more stable (Fig. 5h).

399 In SIM_T_{air} simulation, the air temperature of Kilpisjärvi was replaced by that of
400 Tibet. The average air temperature difference between SIM_T_{air} (-9.83 °C) and CTL (-
401 10.25 °C) was negligible (0.42 °C). In the sensitivity experiment SIM_T_{air}, the water
402 temperature decreased more quickly, and in late October, the lake froze no longer
403 releasing heat into atmosphere. The lake stratification was enhanced, and the water
404 temperature maximum center was ahead about 10 days (Fig. 5c,f).

405 In SIM_q simulation, the specific humidity of Kilpisjärvi was substituted for Tibet.
406 The difference in specific humidity between SIM_q and CTL was 0.38 g kg⁻¹ during

407 ice-covered period. In the sensitivity experiment SIM_q, the simulations were
 408 coincidental to that in CTL, and thus the specific humidity had little effect on the water
 409 temperature (Figs. 5c,i).

410 In conclusion, the stronger downward SR and lower precipitation in the high-
 411 altitude and relatively low-latitude TP played positive roles in the water temperature
 412 warming during the ice-covered period in Ngoring Lake. Less downward LR, lower air
 413 temperature, and larger wind speed did not change the warming trend but affected the
 414 warming amplitude and rate. Specific humidity had no significant influence.



415

416 **Figure 5.** The simulated 3 m daily average water temperature in (a) (d) SIM_{SR},
 417 (a) (g) SIM_{Precip}, (b) (e) SIM_{LR}, (b) (h) SIM_U, (c) (f) SIM_{T_{air}}, (c) (i) SIM_q
 418 sensitivity experiments from November 2015 to June 2016 are compared with the
 419 CTL and the observation, and the change of vertical stratification is shown. The
 420 dotted line represents 3.98 °C.

421

422 6.3 Influences of main physical parameters on water temperature

423 The radiation transfer, which depended on the albedo and extinction coefficient,
 424 played a decisive role in the water temperature. Only influences of A_i , E_i , and E_w
 425 on water temperature simulation were discussed with sensitivity experiments due to less
 426 snow in Tibet. According to previous observations, A_i has observed on TP was mostly
 427 less than 0.12, and the albedo of clear blue ice was only 0.075 (Li et al., 2018). The
 428 range of A_i without snow cover was set as 0.1-0.8 with an interval of 0.1 in SIM_{A_i}

429 experiments.

430 E_i has not been observed on TP, but surveys in Finnish lakes show that the value of
431 bare ice varies between 1-4 m^{-1} , while the value of snow-covered ice can reach 5 m^{-1}
432 (Lei et al., 2011). In SIM_ E_i simulations, E_i was equal to 1-5 m^{-1} with an interval of 1
433 m^{-1} .

434 For the E_w , Zolfaghari et al. (2017) found that the FLake model is particularly
435 sensitive at $E_w \leq 0.5 \text{ m}^{-1}$. Shang et al. (2018) observed that E_i varies from 0.11 to 0.67
436 m^{-1} in a few TP lakes. Therefore, the sensitivity simulations SIM_ E_w were designed in
437 which the E_w varied from 0.1 to 0.5 m^{-1} with an increment step of 0.1 m^{-1} . The
438 experimental settings are shown in Table 3.

439

440 **Table 3.** Numerical sensitivity simulations of parameters affecting the radiative transfer.

Parameter	CTL	SIM_ A_i	SIM_ E_i	SIM_ E_w
A_i	0.25	0.1/0.2/0.3/0.4/0.5 /0.6/0.7/0.8	0.25	0.25
E_i (m^{-1})	2.5	2.5	1.0/2.0/3.0/4.0 /5.0	2.5
E_w (m^{-1})	0.15	0.15	0.15	0.1/0.2/0.3/0.4 /0.5

441

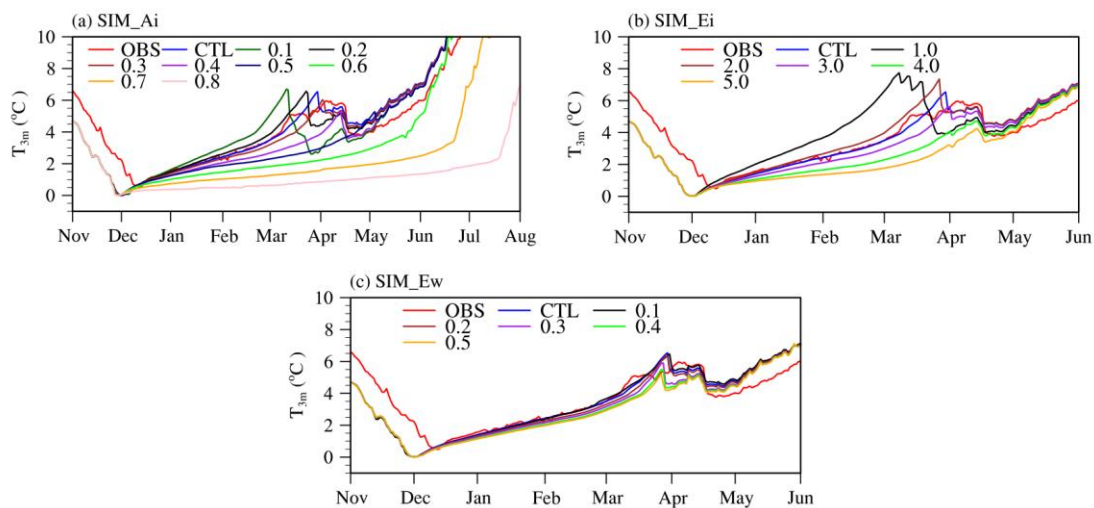
442 In the SIM_ A_i sensitivity experiment, the 3 m water temperature decreased
443 approximately 1 °C when ice albedo increased by 0.1. When the albedo grew to 0.80,
444 the water temperature warming decreased from 4 °C to 2 °C. The increase of ice albedo
445 did not affect the ice formation date but remarkably delayed the ice melting time,
446 accordingly prolonging the ice-covered period. When the albedo increased from 0.1 to
447 0.8, the ice-covered period was extended for 15-30 days for every 0.1 increase (Fig. 6a).

448 In the sensitivity experiment SIM_ E_i , the ice extinction coefficient changes did not
449 all make a continuous rising in water temperature, but the 3 m water temperature
450 decreased by 1-2 °C when ice extinction coefficient increased by 1 m^{-1} (Fig. 6b). The
451 ice absorbed more heat, and the less heat entered the lake water under ice due to the
452 larger ice extinction coefficient.

453 To further discuss influences of A_i and E_i on lake temperature during ice-covered
454 period. The period was divided into two stages Period-A and Period-B in CTL, SIM_ A_i .

455 Period-A ranged from freezing point to T_{md} , Period-B ranged from T_{md} to maximum
 456 temperature (T_m). The duration of Period-A is longer than that of Period-B, and the
 457 temperature heating rate in Period-B ($\sim 0.1 \text{ }^\circ\text{C d}^{-1}$) was 2.5 times greater than that of
 458 Period-A ($\sim 0.04 \text{ }^\circ\text{C d}^{-1}$). The reason was that lake completely covered by ice, and the
 459 inner lake evenly mixed in Period-A, while the ice thickness decreased and the radiation
 460 absorbed by the ice decreased in Period-B. The upper layer absorbed more heat than
 461 the deeper layer, and the upper water temperature increased rapidly. When A_i and E_i
 462 increased, the heating rate decreased and the duration increased in Period-A, the
 463 maximum temperature decreased, the heating rate and duration fluctuate in Period-B.
 464 When $A_i \geq 0.6$, the heating rate during ice-covered period decreases and did not rise to
 465 T_{md} .

466 In the SIM_Ew sensitivity experiment, the water extinction coefficient had just a
 467 little influence on the winter water temperature, 3 m water temperature decreased with
 468 the increase of E_w (Fig. 6c). When only the extinction coefficient of water changed, the
 469 solar radiation entering the water through the ice is unchanged, and so the heat storage
 470 of the lake was unaffected. It is just that the heat distribution in the vertical direction is
 471 changed. The higher the extinction coefficient of water, the more heat was absorbed by
 472 the surface layer and the less heat reached the deep layer. The phenomenon that the 3
 473 m water temperature decreases with the extinction coefficient increasing becomes more
 474 and more obvious in the later stage of ice melting.



475

476 **Figure 6. Comparison of the 3 m simulated daily average water temperature with**
 477 **the observed value under different (a) A_i , (b) E_i , (c) E_w .**

478

479 **6.4 Influences of water temperature on lake-atmosphere exchange**

480 The thermal conditions in an ice-covered lake just before ice melting have a

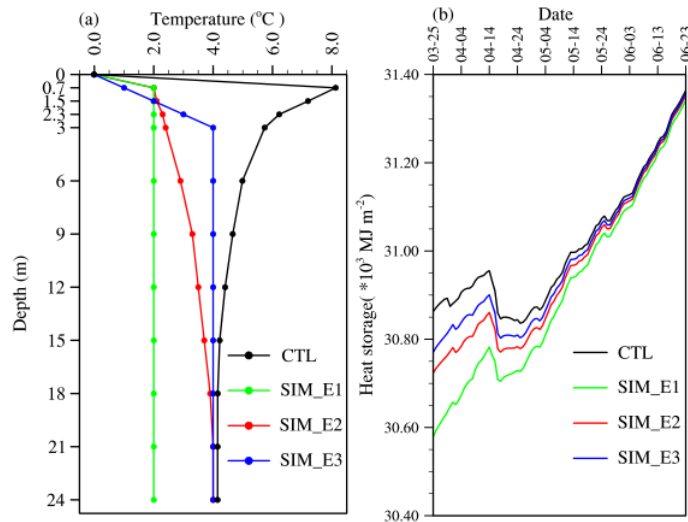
481 significant influence on the air-lake energy exchange. To analyze the effects of lake
482 temperature characteristics on the atmosphere at ice melting, three experiments –
483 SIM_E1, SIM_E2, and SIM_E3 (Table 1) – were set up based on the CTL and the
484 observed lake temperature profile on March 25, 2016, 5 days before ice completely
485 melted (Fig. 7a). The characteristics of the initial water temperature profile were:

- 486 - SIM_E1. The stratification was weak, the first layer temperature was at the
487 melting point, and, from the second layer down, the water temperature was set
488 as 2 °C corresponding to Bangong Co (Wang et al., 2014).
- 489 - SIM_E2. The lake was strongly stratified. The first layer was at the melting
490 point, and the temperature increased linearly reaching T_{md} at the bottom,
491 corresponding to Valkea-Kotinen Lake (Bai et al., 2016).
- 492 - SIM_E3. The temperature of the first layer was at the melting point, and the
493 temperature gradually increased with the depth from the second layer to the
494 middle layer, and the temperature in the middle layer increased to T_{md}
495 corresponding to Thrush Lake (Fang and Stefan, 1996).

496 In CTL, the first layer temperature equal to the freezing/melting point, and the
497 second layer reached the maximum temperature on March 25. The temperature became
498 lower with the deeper layer, until the temperature reached T_{md} .

499 With the different initial temperature profiles, the heat storage was different after
500 ice breakup, and the difference persisted for about two months (Fig. 7b). In CTL, from
501 March 30 to March 31 when ice melted completely, the lake heat storage ranged from
502 30893.02 MJ m⁻² to 30874.51 MJ m⁻², and the heat released was 18.51 MJ m⁻². In the
503 three experiments, from April 1 to April 2 when ice melted completely, the lake heat
504 storage changed from 30657.51 MJ m⁻² to 30651.67 MJ m⁻² in SIM_E1, from 30781.07
505 MJ m⁻² to 30769.91 MJ m⁻² in SIM_E2, and from 30833.28 MJ m⁻² to 30822.42 MJ m⁻²
506 in SIM_E3, and the heat release was 5.84 MJ m⁻², 11.16 MJ m⁻², and 10.86 MJ m⁻²,
507 respectively (Fig. 7b).

508 The heat released was in the form of sensible heat and latent heat, accounting for
509 0.060% (CTL), 0.019% (SIM_E1), 0.036% (SIM_E2), and 0.035% (SIM_E3) of the
510 ice-covered heat storage, respectively. As the initial lake temperature profiles were
511 different before ice complete melting, the ice melted earlier and faster with the higher
512 lake temperature. The lake heat storage increased from March 25 to May 24, and the
513 heat release rate was different under different circumstances. After late May, the heat
514 balance between the lake and the atmosphere was the same, and so the heat storage
515 basically stayed equally after that.

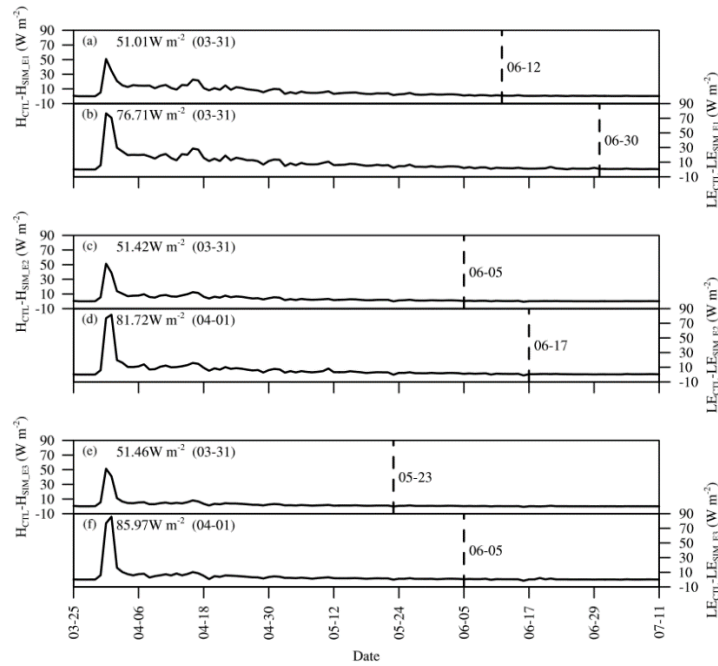


516

517 **Figure 7. (a) The initial water temperature profiles in the model are set on March**
 518 **25, 2016, and the corresponding daily average (b) lake heat storage is simulated.**
 519 **SIM_E1, SIM_E2, and SIM_E3 are three different sensitivity simulations.**

520

521 The lake surface temperature also affected the sensible and latent heat release,
 522 whose differences were calculated between CTL and the three experimental simulations
 523 (Fig. 8). The influence of different initial water temperature profiles started on March
 524 31, that is, when the ice had melted completely in CTL, and when the sensible and latent
 525 differences between CTL and three experimental simulations were less than 0.1 W m^{-2}
 526 for three consecutive days, we judged that the influence had ended. The maximum
 527 differences of the sensible heat (51.0 W m^{-2}) and latent heat (76.7 W m^{-2}) between
 528 SIM_E1 and CTL appeared on March 31 and ended on June 12 and 30, respectively
 529 (Fig. 8a). In SIM_E2 the corresponding numbers were 51.4 W m^{-2} (March 31 to June
 530 5) for sensible heat and 81.7 W m^{-2} (April 1 to June 17) for latent heat (Fig. 8b), and in
 531 SIM_E3 they were 51.5 W m^{-2} (March 31 to May 23) for sensible heat and 86.0 W m^{-2}
 532 (April 1 to June 5) for latent heat (Fig. 8c). Compared with the three lake temperature
 533 experiments, the heating characteristics of Ngoring Lake made the heat release higher
 534 and faster during ice breakup. The duration of heat release difference was from 59 (to
 535 May 23) to 97 (to June 30) days, and for the latent heat release, the situation lasted
 536 about 12-18 days longer than for the sensible heat release.



537

538 **Figure 8. The daily average difference between the sensitivity sensible and latent**
 539 **heat and the CTL under three different initial water temperature profiles in**
 540 **SIM_E1, SIM_E2, and SIM_E3.**

541

542 **7 Conclusions**

543 The analysis demonstrates a significant increase in lake temperature during the ice-
 544 covered period in Ngoring, the largest freshwater lake on the Tibetan Plateau (TP), with
 545 water temperatures exceeding the freshwater maximum density value T_{md} . The heating
 546 is governed by strong solar radiation, the factor differing alpine lakes on the high-
 547 altitude and relatively low-latitude TP from the high-latitude and low-altitude northern
 548 lakes with similar winter air temperature patterns. The one-dimensional lake model
 549 LAKE2.3 successfully captured the major mechanisms of warming and vertical thermal
 550 stratification during the ice-covered period. Compared with MODIS surface
 551 temperature data, the *BIAS*, *RMSE*, and *CC* were 1.42 °C, 3.25 °C, and 0.96,
 552 respectively. The absolute values of *BIAS* and *RMSE* were less than 0.1 °C and 1 °C in
 553 2 m, 9 m, 14 m, and 22 m. The *CC* of simulated and observed water temperature at 2
 554 m, 9 m, and 14 m were as high as 0.98, and the *CC* of simulated and observed water
 555 temperature at 22 m was 0.95.

556 Sensitivity simulations with perturbed local climate data confirmed the decisive
 557 role of subsurface solar radiation in the water temperature rise and demonstrated strong
 558 negative feedback with winter precipitation amount. The downward longwave radiation,
 559 air temperature, and wind speed had only a minor influence on the water temperature.

560 The warming rates and, as a result, the duration of the ice-covered period was
561 sensitive to the physical ice properties: ice albedo and light extinction coefficient both
562 reduced the amount of the subsurface solar radiation. An increase in the albedo of ice
563 reduced the rising trend of water temperature and prolonged the ice season. At the
564 critical albedo of 0.6, the lake water warming decreased obviously and temperature
565 remained stable no more than 3.98 °C. The extinction coefficient of water had just a
566 minor effect on water temperature under the ice.

567 An important consequence of the under-ice solar heat accumulation consisted in
568 increased sensible and latent heat releases in the subsequent open-water phase.
569 According to the model results, the effects on the surface fluxes of Ngoring Lake lasted
570 for 59-97 days after the ice melt and increased the upward latent and sensible surface
571 heat fluxes up to $\sim 80 \text{ W m}^{-2}$ and $\sim 50 \text{ W m}^{-2}$, respectively. Herewith, the phenomenon
572 of under-ice solar heating may have a significant effect on the land-atmosphere
573 interaction on regional scales and has to be accounted for in coupled climate models.

574

575 *Data availability.* The daily precipitation data from Chinese surface stations are
576 available for purchase from the China Meteorological Data Service Center (CMDC,
577 <http://data.cma.cn/en/>). The MODIS LST product is available from National
578 Aeronautics and Space Administration (NASA) (<https://earthdata.nasa.gov/>). ERA5-
579 Land data is available with funding from the European Union's Copernicus Climate
580 Change Service (<https://cds.climate.copernicus.eu/>). Lake temperature data of Ngoring
581 Lake in 2015 and 2016 were uploaded to Zenodo by Georgiy Kirillin
582 (<http://doi.org/10.5281/zenodo.4750910>). The weather observation data of Ngoring
583 Lake can be obtained from the website (<https://nimbus.igb-berlin.de/index.php/s/Moqxgn29DbNFyr8>). The latest version of LAKE model source
584 code is available at zenodo: <https://zenodo.org/record/6353238#.YjCSXi1eNTY>.

586

587 *Author contributions.* MW and LW conceived the study. MW performed the modeling
588 with contributions from VS, LW, and ZL. YZ, RN, and LY processed some data. MW,
589 LW, ML, and GK analyzed the model output. MW wrote the paper, with contributions
590 from all co-authors.

591

592 *Competing interests.* The authors declare that they have no conflict of interest.

593

594 *Acknowledgments.* This study was supported by the National Key Research and
595 Development Program of China (2019YFE0197600) and CAS "Light of West China"
596 Program (E129030101, Y929641001). Victor Stepanenko was supported by Russian
597 Ministry of Science and Higher Education, agreement No. 075-15-2019-1621.

598 **References**

- 599 Bai, Q. X., Li, R. L., Li, Z. J., Leppäranta, M., Arvola, L. and Li, M.: Time-series
600 analyses of water temperature and dissolved oxygen concentration in Lake Valkea-
601 Kotinen (Finland) during ice season, *Ecol Inform*, 36, 181-189, doi:
602 10.1016/j.ecoinf.2015.06.009, 2016.
- 603 Brown, L. C. and Duguay, C. R.: The fate of lake ice in the North American Arctic, *The*
604 *Cryosphere*, 5, 869-892, doi: 10.5194/tc-5-869-2011, 2011.
- 605 Cao, X. W., Lu, P., Leppäranta, M., Arvola, L., Huotari, J., Shi, X. H., Li, G. Y. and Li,
606 Z. J.: Solar radiation transfer for an ice-covered lake in the central Asian arid climate
607 zone, *Inland Waters*, 11, 89-103, doi: 10.1080/20442041.2020.1790274, 2020.
- 608 Dai, Y. J., Wei, N., Huang, A. N., Zhu, S. G., Shangguan, W., Yuan, H., Zhang, S. P. and
609 Liu, S. F.: The lake scheme of the Common Land Model and its performance evaluation
610 (in Chinese), *Chin Sci Bull*, 63, 3002-3021, doi: 10.1360/n972018-00609, 2018.
- 611 Dauginis, A. A. and Brown, L. C.: Recent changes in Pan-Arctic sea ice, lake ice, and
612 snow on/off timing, *The Cryosphere*, 15, 4781-4805, doi: 10.5194/tc-2021-52, 2021.
- 613 Dokulil, M. T.: Predicting summer surface water temperatures for large Austrian lakes
614 in 2050 under climate change scenarios, *Hydrobiologia*, 731, 19-29, doi:
615 10.1007/s10750-013-1550-5, 2013.
- 616 Donlon, C. J., Minnett, P. J., Gentemann, C., Nightingale, T. J., Barton, I. J., Ward, B.,
617 and Murray, M. J.: Toward improved validation of satellite sea surface skin temperature
618 measurements for climate research, *J. Clim.*, 15, 353-369, doi:
619 10.1175/15200442(2002)015<0353:TIVOSS>2.0.CO;2, 2002.
- 620 Efremova, T., Palshin, N. and Zdorovenov, R.: Long-term characteristics of ice
621 phenology in Karelian lakes, *EST J EARTH SCI*, 62, 33-41, doi: 10.3176/earth.2013.04,
622 2013.
- 623 Fang, N., Yang, K., Lazhu, Chen, Y. Y., Wang, J. B. and Zhu, L. P.: Research on the
624 application of WRF-lake Modeling at Nam Co Lake on the Qinghai-Tibetan Plateau,
625 *Plateau Meteorology*, 36, 610-618, doi: 10.7522/j.issn.1000-0534.2016.00038, 2017.
- 626 Fang, X. and Stefan, H. G.: Long-term lake water temperature and ice cover
627 simulations/measurements, *Cold Reg Sci Technol*, 24, 289-304, 1996.
- 628 Gan, G. J. and Liu, Y. B.: Heat storage effect on evaporation estimates of China's largest
629 freshwater lake, *J. Geophys*, 125, 1-14, doi: 10.1029/2019jd032334, 2020.
- 630 Grant, L., Vanderkelen, I., Gudmundsson, L., Tan, Z., Perroud, M., Stepanenko, V.,
631 Debolskiy, A. V., Droppers, B., Janssen, A. B., Woolway, R. I., Choulga, M., Balsamo,
632 G., Kirillin, G., Schewe, J., Zhao, F., Valle, I. V., Golub, M., Pierson, D., Marcé, R.,
633 Seneviratne, S. I. and Thiery, W.: Attribution of global lake systems change to
634 anthropogenic forcing, *Nat. Geosci.*, 14, 1-6, doi: 10.1038/s41561-021-00833-x, 2021.
- 635 Guseva, S., Stepanenko, V., Shurpali, N., Biasi, C., Marushchak, M. E. and Lind, S. E.:

636 Numerical simulation of methane emission from Subarctic Lake in Komi Republic
637 (Russia), *Geography, Environment, Sustainability*, 9, 58-74, doi: 10.15356/2071-
638 9388_02v09_2016_05, 2016.

639 Hardenbicker, P., Viegutz, C., Becker, A., Kirchesch, V., Nilson, E. and Fischer, H.:
640 Water temperature increases in the river Rhine in response to climate change, *Reg
641 Environ Change*, 17, 299-308, doi: 10.1007/s10113-016-1006-3, 2016.

642 Heiskanen, J. J., Mammarella, I., Ojala, A., Stepanenko, V., Erkkilä, K. M., Miettinen,
643 H., Sandström, H., Eugster, W., Leppäranta, M., Järvinen, H., Vesala, T. and Nordbo,
644 A.: Effects of water clarity on lake stratification and lake-atmosphere heat exchange, *J.
645 Geophys*, 120, 7412-7428, doi: 10.1002/2014jd022938, 2015.

646 Hersbach, H., Bell, B., Berrisford, P., Hirahara, S., Horányi, A., Muñoz-Sabater, J.,
647 Nicolas, J., Peubey, C., Radu, R., Schepers, D., Simmons, A., Soci, C., Abdalla, S.,
648 Abellan, X., Balsamo, G., Bechtold, P., Biavati, G., Bidlot, J., Bonavita, M., Chiara, G.,
649 Dahlgren, P., Dee, D., Diamantakis, M., Dragani, R., Flemming, J., Forbes, R., Fuentes,
650 M., Geer, A., Haimberger, L., Healy, S., Hogan, R. J., Hólm, E., Janisková, M., Keeley,
651 S., Laloyaux, P., Lopez, P., Lupu, C., Radnoti, G., Rosnay, P., Rozum, I., Vamborg, F.,
652 Villaume, S. and Thépaut, J. N.: The ERA5 global reanalysis, *Q J R Meteorol Soc*, 146,
653 1999-2049, doi: 10.1002/qj.3803, 2020.

654 Huang, A. N., Lazhu, Wang, J. B., Dai, Y. J., Yang, K., Wei, N., Wen, L. J., Wu, Y., Zhu,
655 X. Y., Zhang, X. D. and Cai, S. X.: Evaluating and improving the performance of three
656 1-D lake models in a large deep lake of the central Tibetan Plateau, *J. Geophys*, 124,
657 3143-3167, doi: 10.1029/2018JD029610, 2019.

658 Kirillin, G. B., Aslamov, I., Kozlov, V., Zdorovenov, R., and Granin, N.: Turbulence
659 in the stratified boundary layer under ice: observations from Lake Baikal and a new
660 similarity model, *Hydrol. Earth Syst. Sci.*, 24, 1691-1708, doi: 10.5194/hess-24-1691-
661 2020, 2020.

662 Kirillin, G. B., Aslamov, I., and Leppäranta, M.: Turbulent mixing and heat fluxes under
663 lake ice: the role of seiche oscillations, *Hydrol. Earth Syst. Sci.*, 22, 6493-6504, doi:
664 10.5194/hess-22-6493-2018, 2018.

665 Kirillin, G. B., Leppäranta, M., Terzhevik, A., Granin, N., Bernhardt, J., Engelhardt, C.,
666 Efremova, T., Golosov, S., Palshin, N., Sherstyankin, P., Zdorovenova, G. and
667 Zdorovenov, R: Physics of seasonally ice-covered lakes: a review, *Aquat Sci*, 74, 659-
668 682, doi: 10.1007/s00027-012-0279-y, 2012.

669 Kirillin, G. B., Wen, L. J. and Shatwell, T.: Seasonal thermal regime and climatic trends
670 in lakes of the Tibetan highlands, *Hydrol Earth Syst Sci*, 21, 1895-1909, doi:
671 10.5194/hess-21-1895-2017, 2017.

672 Kirillin, G. B., Forrest, A. L., Graves, K. E., Fischer, A., Engelhardt, C. and Laval, B.
673 E.: Axisymmetric circulation driven by marginal heating in ice-covered lakes, *Geophys*

674 Res Lett, 42, 2893-2900, doi: 10.1002/2014gl062180, 2015.

675 Kirillin, G. B., Shatwell, T. and Wen, L. J.: Ice-covered lakes of Tibetan Plateau as solar
676 heat collectors, Geophys. Res. Lett., 48, 1-12, doi: 10.1029/2021gl093429, 2021.

677 Lazhu, Yang, K., Hou, J. Z., Wang, J. B., Lei, Y. B., Zhu, L. P., Chen, Y. Y., Wang, M.
678 D. and He, X. G.: A new finding on the prevalence of rapid water warming during lake
679 ice melting on the Tibetan Plateau, Sci. Bull., 66, 2358-2361, doi:
680 10.1016/j.scib.2021.07.022, 2021.

681 Lazhu, Yang, K., Wang, J. B., Lei, Y. B., Chen, Y. Y., Zhu, L. P., Ding, B. H. and Qin,
682 J.: Quantifying evaporation and its decadal change for Lake Nam Co, central Tibetan
683 Plateau, J. Geophys, 121, 7578-7591, doi: 10.1002/2015jd024523, 2016.

684 Lei, R. B., Leppäranta, M., Erm, A., Jaatinen, E. and Pärn, O.: Field investigations of
685 apparent optical properties of ice cover in Finnish and Estonian lakes in winter 2009,
686 EST J EARTH SCI, 60, 50-64, doi: 10.3176/earth.2011.1.05, 2011.

687 Leppäranta, M.: Freezing of lakes and the evolution of their ice cover, Germany:
688 Springer Science & Business Media, 2014.

689 Leppäranta, M., Lindgren, E. and Shirasawa, K.: The heat budget of Lake Kilpisjärvi
690 in the Arctic tundra, Hydrology Research, 48, 969-980, doi: 10.2166/nh.2016.171, 2017.

691 Leppäranta, M., Lindgren, E., Wen, L. J. and Kirillin, G.: Ice cover decay and heat
692 balance in Lake Kilpisjärvi in Arctic tundra, J Limnol, 78, doi:
693 10.4081/jlimnol.2019.1879, 2019.

694 Li, G. C., Liu, Z. G., Zhang, M., Li, J., Pi, K., Xiong, Y. and Xu, J.: A preliminary study
695 of effects of warming on the nutrients dynamic in sediment of hypereutrophic shallow
696 lake, Acta Ecologica Sinica, 35, 4016-4025, doi: 10.5846/stxb201309102244, 2015a.

697 Li, Z. G., Ao, Y. H., Lyu, S. H., Lang, J. H., Wen, L. J., Stepanenko, V., Meng, X. H.
698 and Zhao, L.: Investigation of the ice surface albedo in the Tibetan Plateau lakes based
699 on the field observation and MODIS products, J Glaciol, 64, 506-516, doi:
700 10.1017/jog.2018.35, 2018.

701 Li, Z. G., Lyu, S. H., Ao, Y. H., Wen, L. J., Zhao, L. and Wang, S. Y.: Long-term energy
702 flux and radiation balance observations over Lake Ngoring, Tibetan Plateau, Atmos Res,
703 155, 13-25, doi: 10.1016/j.atmosres.2014.11.019, 2015b.

704 Li, Z. G., Lyu, S. H., Wen, L. J., Zhao, L., Ao, Y. H. and Meng, X. H.: Study of freeze-
705 thaw cycle and key radiation transfer parameters in a Tibetan Plateau lake using
706 LAKE2.0 model and field observations, J Glaciol, 45, 1-16, doi: 10.1017/jog.2020.87,
707 2020.

708 Muñoz-Sabater, J., Dutra, E., Agustí-Panareda, A., Albergel, C., Arduini, G., Balsamo,
709 G., Bousssetta, S., Choulga, M., Harrigan, S., Hersbach, H., Martens, B., Miralles, D.
710 G., Piles, M., Rodríguez-Fernández, N. J., Zsoter, E., Buontempo, C. and Thépaut, J.-
711 N.: ERA5-Land: A state-of-the art global reanalysis dataset for land applications, Earth

712 Syst. Sci. Data, 1-50, doi: 10.5194/essd-2021-82, 2021.

713 Nordbo, A., Launiainen, S., Mammarella, I., Leppäranta, M., Huotari, J., Ojala, A. and
714 Vesala, T.: Long-term energy flux measurements and energy balance over a small boreal
715 lake using eddy covariance technique, *J. Geophys. Res. Atmos.*, 116, 1-17, doi:
716 10.1029/2010jd014542, 2011.

717 Ramp, C., Delarue, J., Palsboll, P. J., Sears, R. and Hammond, P. S.: Adapting to a
718 warmer ocean--seasonal shift of baleen whale movements over three decades, *PLoS*
719 *One*, 10, 1-15, doi: 10.1371/journal.pone.0121374, 2015.

720 Rösner, R. R., Müller-Navarra, D. C. and Zorita, E.: Trend analysis of weekly
721 temperatures and oxygen concentrations during summer stratification in Lake Plußsee:
722 A long-term study, *Limnol. Oceanogr.*, 57, 1479-1491, doi: 10.4319/lo.2012.57.5.1479,
723 2012.

724 Shang, Y. X., Song, K. S., Jiang, P., Ma, J. H., Wen, Z. D. and Zhao, Y.: Optical
725 absorption properties and diffuse attenuation of photosynthetic active radiation for
726 inland waters across the Tibetan Plateau, *Journal of Lake Sciences*, 30, 802-811, doi:
727 10.18307/2018.0322, 2018.

728 Sharma, S., Blagrove, K., Magnuson, J. J., O'Reilly, C. M., Oliver, S., Batt, R. D.,
729 Magee, M. R., Winslow, L. and Woolway, R. I.: Widespread loss of lake ice around the
730 Northern Hemisphere in a warming world, *Nature Clim. Change.*, 9, 227-231, doi:
731 10.1038/s41558-018-0393-5, 2019.

732 Sharma, S., Meyer, M. F., Culpepper, J., Yang, X., Hampton, S., Berger, S. A., Brousil,
733 M. R., Fradkin, S. C., Higgins, S. N., Jankowski, K. J., Kirillin, G., Smits, A. P.,
734 Whitaker, E. C., Yousef, F. and Zhang, S.: Integrating perspectives to understand lake
735 ice dynamics in a changing world, *J. Geophys. Res. Biogeosci.*, 125, 1-18, doi:
736 10.1029/2020jg005799, 2020.

737 Shen, D. F., Li, S. J., Jiang, Y. J. and Chen, W.: Water environment characteristics and
738 regional climate response of typical lakes in Yellow River headwater area, *J. Arid*
739 *Environ.*, 26, 91-97, doi: 10.13448/j.cnki.jalre.2012.07.030, 2012.

740 Song, X. Y., Wen, L. J., Li, M. S., Du, J., Su, D. S., Yin, S. C. and Lv, Z.: Comparative
741 study on applicability of different lake models to typical lakes in Qinghai-Tibetan
742 Plateau, *Plateau Meteorology*, 39, 213-225, doi: 10.7522/j.issn.1000-0534.2019.00102,
743 2020.

744 Stepanenko, V., Mammarella, I., Ojala, A., Miettinen, H., Lykosov, V. and Vesala, T.:
745 LAKE 2.0: a model for temperature, methane, carbon dioxide and oxygen dynamics in
746 lakes, *Geosci Model Dev*, 9, 1977-2006, doi: 10.5194/gmd-9-1977-2016, 2016.

747 Stepanenko, V. and Lykosov, V. N.: Numerical modeling of heat and moisture transfer
748 processes in a system lake soil, *Russ. Meteorol. Hydrol.*, 3, 95-104, 2005.

749 Stepanenko, V., Machul'skaya, E. E., Glagolev, M. V. and Lykosov, V. N.: Numerical

750 modeling of methane emissions from lakes in the permafrost zone, *IZV ATMOS*
751 *OCEAN PHY+*, 47, 252-264, doi: 10.1134/s0001433811020113, 2011.

752 Stepanenko, V., Repina, I. A., Ganbat, G. and Davaa, G.: Numerical simulation of ice
753 cover of saline lakes, *IZV ATMOS OCEAN PHY+*, 55, 129-138, doi:
754 10.1134/s0001433819010092, 2019.

755 Tavares, M., Cunha, A., Motta-Marques, D., Ruhoff, A., Cavalcanti, J., Fragoso, C.,
756 Martín Bravo, J., Munar, A., Fan, F. and Rodrigues, L.: Comparison of methods to
757 estimate Lake-Surface-Water temperature using Landsat 7 ETM+ and MODIS imagery:
758 Case study of a large shallow subtropical lake in Southern Brazil, *Water*, 11, 1-21, doi:
759 10.3390/w11010168, 2019.

760 Tolonen, A.: Application of a bioenergetics model for analysis of growth and food
761 consumption of subarctic whitefish *Coregonus lavaretus* (L.) in Lake Kilpisjärvi,
762 Finnish Lapland, *Hydrobiologia*, 390, 153-169, doi: 10.1023/A:1003525008870, 1998.

763 Wan, W., Long, D., Hong, Y., Ma, Y. Z., Yuan, Y., Xiao, P. F., Duan, H. T., Han, Z. Y.
764 and Gu, X. F.: A lake data set for the Tibetan Plateau from the 1960s, 2005, and 2014,
765 *Sci. Data.*, 3, 1-13, doi: 10.1038/sdata.2016.39, 2016.

766 Wan, Z., Zhang, Y., Zhang, Q. and Li, Z. L.: Quality assessment and validation of the
767 MODIS global land surface temperature, *Int J Remote Sens*, 25, 261-274, doi:
768 10.1080/0143116031000116417, 2004.

769 Wang, M. D., Hou, J. Z. and Lei, Y. B.: Classification of Tibetan lakes based on
770 variations in seasonal lake water temperature, *Chinese Science Bulletin*, 59, 4847-4855,
771 doi: 10.1007/s11434-014-0588-8, 2014.

772 Wang, M. X., Wen, L. J., Li, Z. G. and Su, D. S.: Study on the warming characteristics
773 during the ice-covered period of Ngoring Lake in the Qinghai-Xizang Plateau, *Plateau*
774 *Meteorology*, 40, 965-976, doi: 10.7522/j.issn.1000-0534.2020.00112, 2021.

775 Weitere, M., Vohmann, A., Schulz, N., Linn, C., Dietrich, D. and Arndt, H.: Linking
776 environmental warming to the fitness of the invasive clam *Corbicula fluminea*, *Glob*
777 *Chang Biol*, 15, 2838-2851, doi: 10.1111/j.1365-2486.2009.01925.x, 2010.

778 Wen, L. J., Lyu, S. H., Kirillin, G., Li, Z. G. and Zhao, L.: Air-lake boundary layer and
779 performance of a simple lake parameterization scheme over the Tibetan highlands,
780 *Tellus A*, 68, 1-15, doi: 10.3402/tellusa.v68.31091, 2016.

781 Wen, L. J., Wang, C., Li, Z. G., Zhao, L., Lyu, S. H. and Chen, S. Q.: Thermal responses
782 of the largest freshwater lake in the Tibetan Plateau and its nearby saline lake to climate
783 change, *Remote Sens.*, 14, 1-19, doi: 10.3390/rs14081774, 2022.

784 Wu, Y., Huang, A. N., Lazhu, Yang, X. Y., Qiu, B., Zhang, Z., Q. and Zhang X., D.:
785 Numerical study of the thermal structure and circulation in a large and deep dimictic
786 lake over Tibetan Plateau, *J. Geophys. Res. Oceans*, 126, 1-22, doi:
787 10.1029/2021jc017517, 2021.

788 Yang, B., Wells, M. G., McMeans, B. C., Dugan, H. A., Rusak, J. A., Weyhenmeyer, G.
789 A., Brentrup, J. A., Hrycik, A. R., Laas, A., Pilla, R. M., Austin, J. A., Blanchfield, P. J.,
790 Carey, C. C., Guzzo, M. M., Lottig, N. R., MacKay, M. D., Middel, T. A., Pierson, D.
791 C., Wang, J. and Young, J. D.: A new thermal categorization of ice-covered lakes,
792 *Geophys. Res. Lett.*, 48, 1-11, doi: 10.1029/2020gl091374, 2021.

793 Zhang, G. Q., Luo, W., Chen, W. F. and Zheng, G. X.: A robust but variable lake
794 expansion on the Tibetan Plateau, *Sci. Bull.*, 64, 1306-1309, doi:
795 10.1016/j.scib.2019.07.018, 2019.

796 Zolfaghari, K., Duguay, C. R. and Kheyrollah Pour, H.: Satellite-derived light
797 extinction coefficient and its impact on thermal structure simulations in a 1-D lake
798 model, *Hydrol Earth Syst Sci*, 21, 377-391, doi: 10.5194/hess-2016-82, 2017.
799